

Electrochemical Studies and Molecular Dynamics Simulation of the Interaction between Accelerators and Cu Surface During the Electroplating Process

Zhongliang Xiao, Zhaohua Zhou, Liubin Song, DaoXin Wu*, Chao Zeng, Zhong Cao

Hunan Provincial Key Laboratory of Materials Protection for Electric Power and Transportation, School of Chemistry and Biological Engineering, Changsha University of Science and Technology, Hunan Changsha 410114, PR China.

*E-mail: xiaozhongliang@163.com

Received: 2 January 2019 / Accepted: 4 March 2019 / Published: 10 April 2019

Accelerators are crucial for electroplating in the electronics industry. In this research, the electrochemical behavior of two accelerators, 3-(benzothiazolyl-2-mercapto)-propyl-sulfonic acid sodium salt (ZPS) and bis(3-sulfopropyl) disulfide (SPS), during Cu electrodeposition was analyzed using electrochemical techniques. Meanwhile, the adsorption behavior of the two accelerators on Cu(111) was also studied using molecular dynamics (MD) simulation, which predicts the preferable reaction sites for nucleophilic or electrophilic attack and the corresponding interactions based on density functional theory. The MD results showed that ZPS could be adsorbed on the Cu(111) firmly through the thiouronium group and a benzothiazolyl group, whereas the SPS was adsorbed through the thiouronium group. Moreover, the accelerating efficiency of these two accelerators was closely related to the frontier molecule orbital density distributions and Fukui indices.

Keywords: copper electroplating; electrochemistry; MD simulation; ZPS; SPS

1. INTRODUCTION

With the miniaturization and high-density and high-speed development of electronic terminal products, the high-density interconnect (HDI) multilayer board is becoming increasingly popular in the production of printed circuit boards (PCBs) [1-3]. In this technology, the through/blind vias are favorably used in the connection between boards. Recently, additional requirements for copper electroplating additives have been demanded to achieve the electroplating technique from bottom to up filling [4-6]. In terms of the accelerator, Wang [7] studied thiazolanyl-dithiopropene sulfonate sodium (SH110) as a single additive and performed the electroplating filling of via with high aspect ratio under low-current

conditions. The via filling can be achieved by using the performance characteristics of SH110, which exerts a restraining function at high flow rate and an accelerating function at low flow rate [8]. However, some problems such as microvia breakage and microvia electroplating failure would still occur in the HDI product despite using the existing accelerator. Therefore, new inexpensive accelerators with excellent properties are urgently needed. However, acquiring novel additives merely based on traditional methods, which are time consuming and inefficient, is challenging. In addition, the mechanism of the accelerator should be studied in further detail. Until now, the bottom-up filling for microvia has been explained using the curvature-enhanced accelerator coverage (CEAC) mechanism proposed by Moffat [9-11]. According to the CEAC mechanism [12-15], the shape evolution of the area covered by the accelerator leads to different copper deposition rates. This theory is based on the results of common morphology and structure analysis, without the support of in-depth molecular level theories. Chen [15] applied the molecular orbital and Fukui indices of the quantum chemical computing inhibitor diketopyrrolopyrrole and its derivatives and suggested that “=O” was the most susceptible moiety anchored on the Cu surface. Lei [17] used 6-dimethyl-2-mercaptopyrimidine and three tetrazoliums as leveler and compared their energy gaps (ΔE) between the highest occupied molecular orbital (HOMO) and the lowest unoccupied molecular orbital (LUMO) using density functional theory (DFT). Xia [18] studied the corrosion inhibition performance of imidazoline structures through molecular dynamics (MD) simulation and demonstrated that two imidazoline derivatives can be adsorbed on the Fe surface through the imidazoline ring and heteroatoms with the alkyl chain approximately perpendicular to the surface. As a widely studied accelerator, SPS has played an important role in synergy and antagonism effect with other components [19]. However, the surface adsorption performance and mechanism of SPS and a new accelerator ZPS with Cu have not been studied at the molecular level by means of orbital energy distribution and MD simulation.

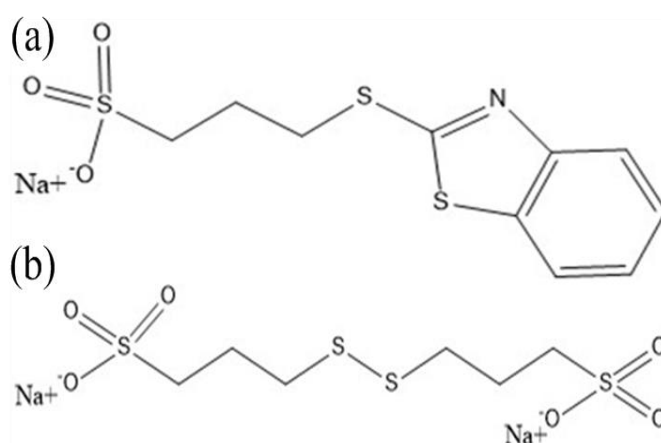


Figure 1. Molecular structures of (a) ZPS and (b) SPS

In this work, we investigated different conditions of ZPS and SPS to determine their optimized concentrations for copper electroplating. The molecular structures of ZPS and SPS are shown in Fig. 1. The electrochemical behaviors of additives were characterized using cyclic voltammetry (CV) and polarization analysis [17]. The adsorption behavior, energy fluctuations, and quantum calculations of accelerators and Cu surface were obtained to reveal the interaction between additives and Cu(111)

surface. This study offers some theoretical insights into the design and synthesis of new additives for electroplating.

2. EXPERIMENTAL

2.1. Electroplating

Metallizing the holes of multilayer PCB involves two steps: formation of a thin conductive layer using copper electroless deposition process and thickening of the copper layer by electroplating.

The PCB was electroplated using the DC method, and current density was 20 ASF. The thickness of the microvia metallized by copper electroless deposition process was 2–3 μm [19]. Phosphoric copper was used as an anode (P 0.03–0.065 wt.%). The dimension of the PCB sample was $1 \times 2 \text{ cm}^2$ and directly placed in 200 mL plating solution. Constant agitation was applied during electroplating by means of continuously flowing air bubbles to ensure efficient transfer. The electroplating solution used for microvia filling experiments was composed of 65 g/L $\text{CuSO}_4 \cdot 5\text{H}_2\text{O}$, 220 g/L H_2SO_4 , 20 mg/L suppressor and leveler, and 60 mg/L Cl^- .

2.2. Electrochemical procedures

CV and Potentiodynamic polarization experiments were performed using a CHI760D Electrochemical Workstation (Shanghai Chenhua, China) with a standard three-electrode cell, which consisted of a mercury sulfate electrode as a reference electrode, platinum foil as a counter electrode, and glassy carbon electrode (GCE, Teflon coated) as a working electrode. Before the plating process, GCE was polished to the mirror surface on the wetted fine fabrics, which were sprinkled with $\alpha\text{-Al}_2\text{O}_3$ powder with different particle diameters. After ultrasonic cleaning with ethanol and repeated treatment by CV in 0.5 mol/L H_2SO_4 , the samples were finally cleaned with distilled water.

Electrochemical experiments were conducted from the open circuit potential to -1.0 V at a constant scan rate of 10 mV/s [21]. In the polarization test, pre-plated copper was used for balance potential as a base layer and then scanned from -0.05 V to 0.12 V at a constant scan rate of 10 mV/s.

2.3. Coating surface properties

In this experiment, the bonding strength was based on GB/T5270-2005. 3M tape with a width of 25 mm and a bonding strength of 8N was used for Cu layer peeling experiment [22]. According to the amount of metal powder that adhered to the adhesive tape, the bonding force was evaluated and divided into five levels. The level with no metal layer or metal powder that peeled off from the adhesive tape was designated as Level 5.

Level 5: No metal layer peeling or metal powder on the adhesive tape.

- Level 4: Adhesive tape has a trace of serrated metal layer or metal powder peeling off.
 Level 3: Adhesive tape has a small amount of serrated metal layer or powder peeling off.
 Level 2: Adhesive tape has a large number of serrated metal layer or metal powder peeling off.
 Level 1: Most areas on the adhesive tape have serrated metal layer or metal powder peeling off.

2.4. Molecular simulation

Geometric structure optimization of molecules was performed using DMol3 Tools [23]. After the optimization, the energies of the HOMO and LUMO were calculated by DFT using the B3LYP method and DND basis set to obtain the preferred reaction sites [8,24,25]. In addition, SCF tolerance was 1.0×10^{-5} .

The ionization potential (IE), and the electron affinity (EA), can be dominated by the following two equations, respectively,

$$IE = -E_{HOMO} \quad (1)$$

$$EA = -E_{LUMO} \quad (2)$$

The absolute hardness, η , and the global chemical softness S were given in the following equations [26].

$$\eta = \frac{IE-EA}{2} \quad (3)$$

$$S = 2\eta^{-1} = \frac{1}{IE-EA} \quad (4)$$

The local reactivity of different heteroatom-protonated accelerators was analyzed by evaluating the Fukui indices. The Fukui indices (f^+ and f^-) were calculated using DFT to evaluate the electron gain and donation abilities [27-29]. The Fukui indices were defined as

$$f^+ = q^{N+1} - q^N \text{ (nucleophilic attack)} \quad (5)$$

$$f^- = q^N - q^{N-1} \text{ (electrophilic attack)} \quad (6)$$

where q was the electronic population of the atom in a molecule.

Forcite module calculations were carried out at the same theoretical levels to simulate the MD of interaction between the accelerator and the Cu(111) surface [30-32]. The temperature in the simulation was fixed at 298 K with COMPASS force field for geometric optimization. The molecules were first optimized to pose the most stable configuration. Then, the box was optimized to a favorable geometry. The supercell range was set to $U = 8$, $V = 3$. The dynamic simulations were performed on the conditions of NVT ensemble with a step time of 0.1 fs and simulation time of 2000 ns. Figs. 6 and 7 show the amorphous boxes consisting of ZPS and SPS molecules. The interaction energy of the Cu surface with ZPS and SPS was calculated according to the following equation:

$$E_{binding} = E_{complex} - (E_{Cu} + E_{additive}) \quad (7)$$

where $E_{complex}$ is the total energy of the Cu crystal together with the adsorbed accelerator molecule and E_{Cu} and $E_{additive}$ are the total energy of the Cu crystal and accelerator molecule, respectively. The binding energy was the negative value of the interaction energy [33], $E_{binding} = -E_{Cu-additive}$.

3. RESULTS AND DISCUSSION

3.1. SEM images

The microvia's surface morphologies formed from copper electroplating in different additive concentrations were examined using SEM (Fig. 2).

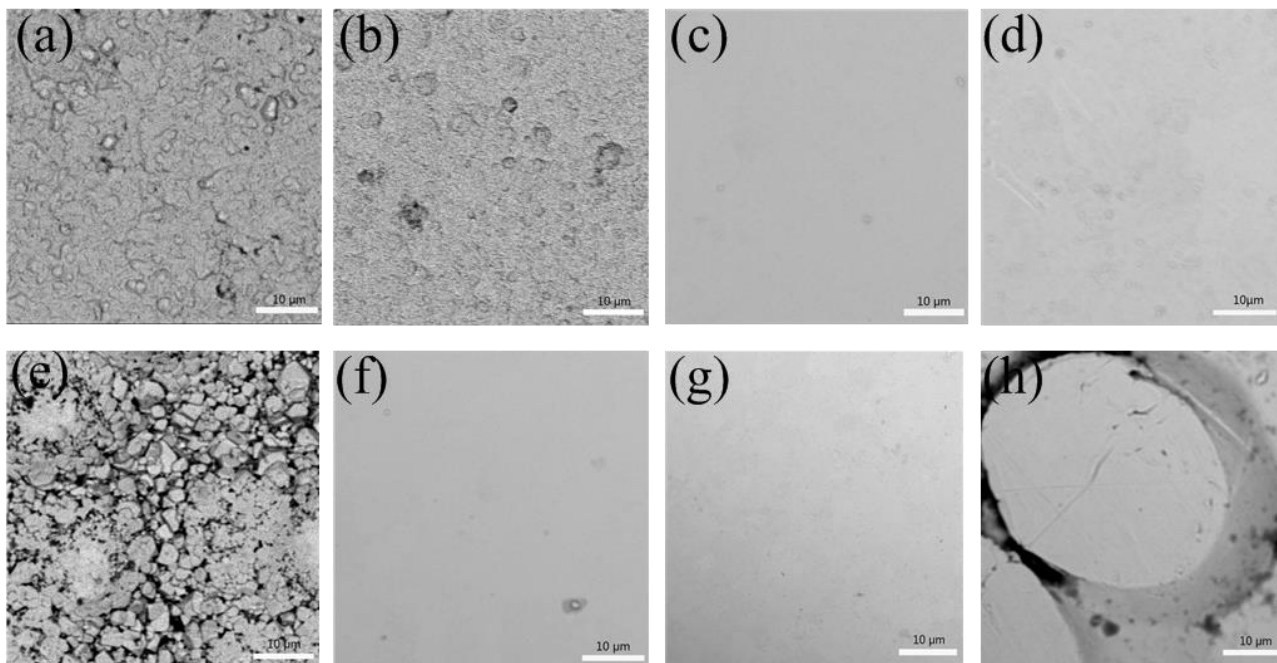


Figure 2. SEM images of ZPS: (a) 0.0, (b) 1.0, (c) 2.0, and (d) 3.0 mg/L. SEM images of SPS: (e) 0.0, (f) 1.0, (g) 2.0, and (h) 3.0 mg/L.

The SEM images show that at a constant plating current density, no significant difference in the surface morphology could be found in copper materials deposited from a 1.0 mg/L bath (Fig. 2f) and from a 2.0 mg/L SPS solution (Fig. 2g). However, the surface was obviously rougher and more porous for copper plated from a 3.0 mg/L SPS solution (Fig. 2h). The adsorption property of the copper material plated from a bath containing 2.0 mg/L SPS was better than that plated from a bath containing 2.0 mg/L ZPS solution. The ZPS surface of the copper was rougher and more porous than that of SPS. The results showed that the surface roughness and surface porosity of the copper deposits changed along with the copper electroplating parameters such as bath composition and concentration [34]. As shown in Fig. 2b and 2h, another factor that needs to be addressed was the different critical concentrations where the transition from “voiding” to “no voiding” occurs. According to a previous study [13], additive incorporation is governed by the delicate balance between the additive surface coverage and the component interaction in Cu plating. Typically, the hydrogen evolution was consequently improved in both ZPS and SPS bath. Thus, the addition of 3.0 mg/L of ZPS and 2.0 mg/L of SPS enabled the copper grain distribution to become more uniform, which improved the dispersion ability of the plating solution

at the middle and high current density and resulted in a wide operating window range and uniform and meticulous copper coating.

3.2. Potentiodynamic polarization of the ZPS and SPS additives

Fig. 3 shows the polarization curves of GCE in different ZPS and SPS electrolyte concentrations. ZPS has inhibition effects on the surface diffusion of copper ion at low concentration, lowering the current density and causing two-dimensional copper growth.

With the increase in ZPS concentration, the deposition current on the coating surface increased, which improved the stability of the PCB. This finding is consistent with a previous study by Chena [30], who described ZPS as an accelerant for Cu deposition. Current density was obtained by slope fitting of Butler–Volmer treatment [18]. In addition, the exchange currents of 2.0 mg/L of SPS and 3.0 mg/L of ZPS were the largest, and the slope was significantly larger than that in other concentrations. According to the obtained results, it can be observed that the Tafel slope increases moderately in the presence of ZPS and SPS, the larger the slope, the larger the current increases under the same potential change, which can improve the distribution of current in the pore and reflects the acceleration of the accelerator in the bath. The surface binding force of the plating layer is shown in Table 1. Level 4 indicates that the adhesive tape has a trace of serrated metal layer or metal powder peeling off. Level 3 represents that the adhesive tape has a small amount of serrated metal or powder layer peeling. After the addition of additives, the surface binding force of the plating layer was obviously enhanced.

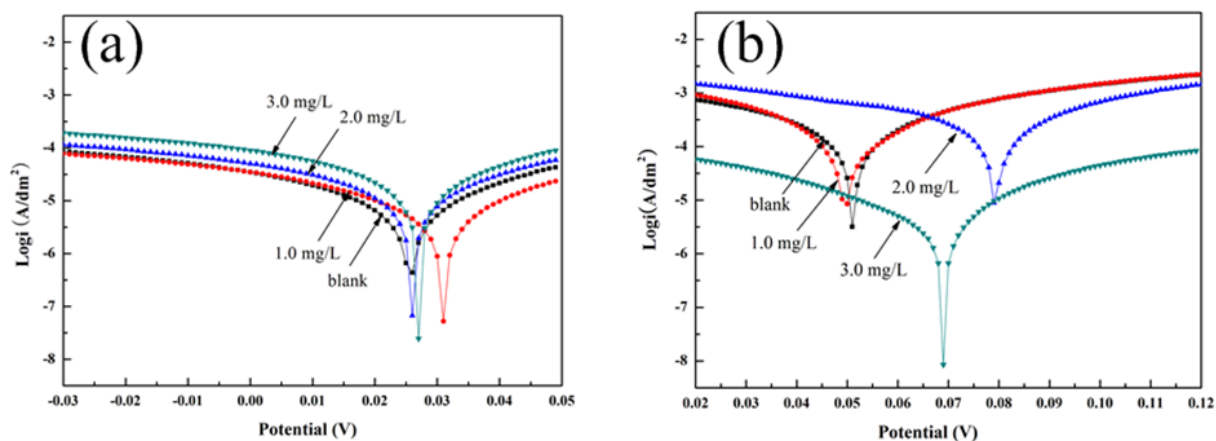


Figure 3. Polarization behavior curve of different concentrations at a scan rate of 10 mV s⁻¹: (a) ZPS and (b) SPS.

Table 1. Potentiodynamic polarization and bonding force parameters for copper strip at different concentrations in the electrolyte.

Accelerator	Concentration (mg/L)	Exchange current density(A/dm ²)	Binding force
ZPS	0.0	8.593×10^{-6}	Level 3
	1.0	9.956×10^{-6}	Level 4
	2.0	1.668×10^{-5}	Level 4
	3.0	1.546×10^{-5}	Level 4
SPS	0.0	8.816×10^{-4}	Level 3
	1.0	12.975×10^{-4}	Level 4
	2.0	9.559×10^{-4}	Level 4
	3.0	7.772×10^{-4}	Level 4

3.3. CV curves of the ZPS and SPS additives on Cu surface

CV is a common electrochemical research method used for studying the metal electrodeposition process. Fig.4 shows that the curves measured by negative potential scanning and positive scanning do not coincide, indicating a reversible reaction. The reason for this phenomenon was that the additives adsorbed on the electrode surface underwent adsorption when the electrodes were constantly moving during the desorption process, and the two processes take some time, so the current of the backsweep changed with the previous one. The addition of SPS and ZPS negatively shifted the deposition peak potential of copper, indicating that the additive can promote copper deposition.

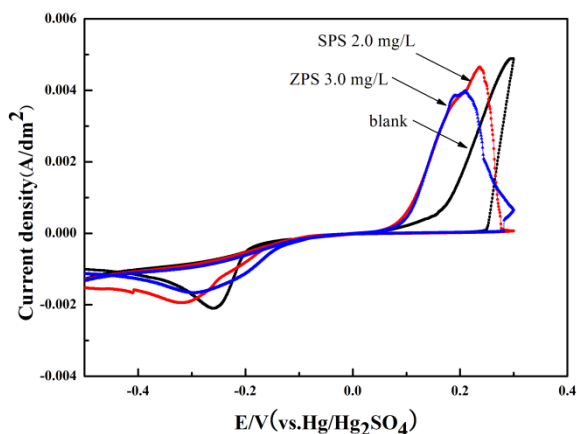


Figure 4. Cyclic voltammograms recorded in blank solution, 2.0 mg/L of SPS, and 3.0 mg/L ZPS.

The electrochemical experiments and surface morphologies showed that the best concentrations of SPS and ZPS were 2.0 and 3.0 mg/L, respectively. However, the polarization became weaker with increasing SPS and ZPS concentration. This finding indicated that higher concentrations of SPS and ZPS

accelerated the deposition. These results can be explained by the fact that mercaptan groups in accelerators are adsorbed on the cathode copper surface and that their sulfonic anions bind to the copper ions and then interact with chlorine ions adsorbed on the surface of the cathode. These findings were consistent with the results of subsequent quantum chemical calculations.

3.4. Molecular simulation

To determine the strength of accelerators, we performed MD simulations in water solution. As a result, the thermodynamic information of accelerators was obtained. The MD simulation was performed to study the adsorption behavior of the two accelerators on the Cu(111) surface [35]. The system achieves equilibrium only if both the temperature and energy reach balance. Figs. 5 and 6 show the initial and final adsorption of ZPS and SPS molecules on the copper surface. Fig. 7 shows that the system tends to reach temperature equilibrium. Fig. 8 shows the energy fluctuation curves of ZPS and SPS molecules simulated in water solution.

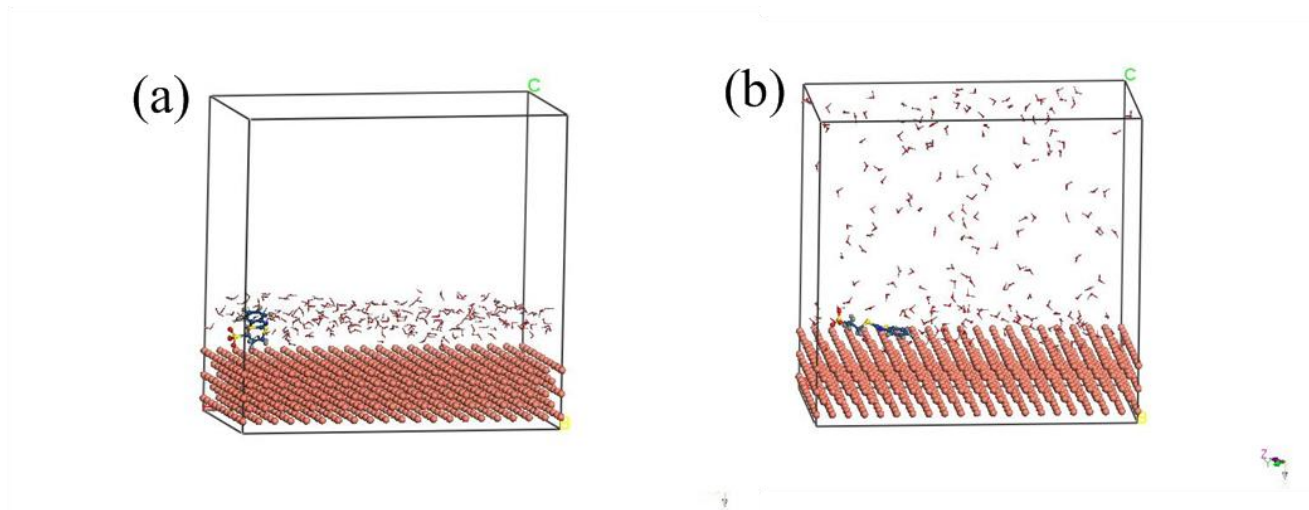


Figure 5. Model of ZPS molecule adsorbed on the Cu(111) surface: (a) initial and (b) final.

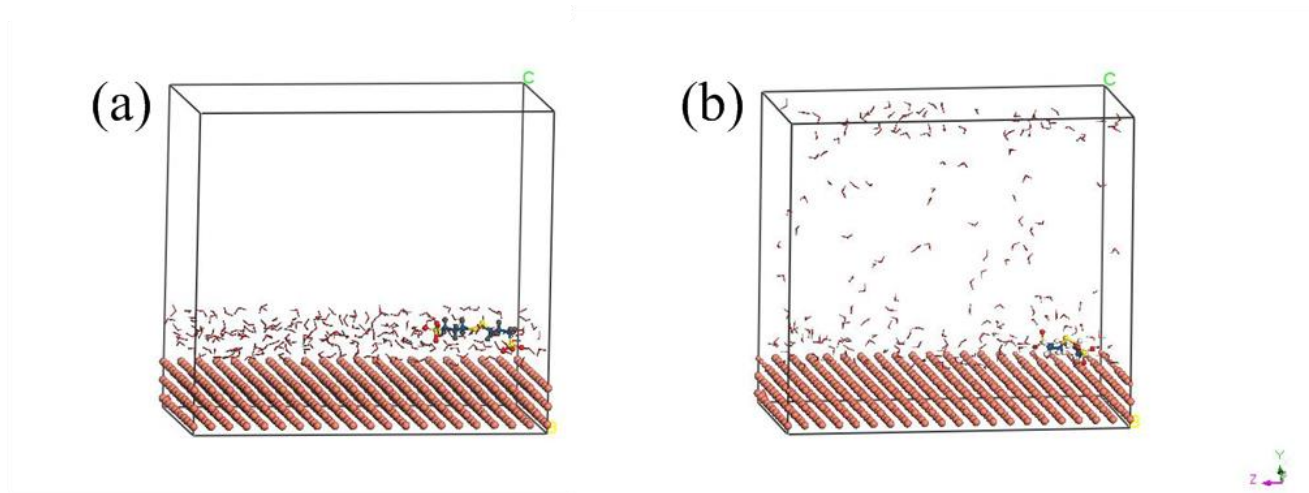


Figure 6. Model of ZPS molecule adsorbed on the Cu(111) surface: (a) initial and (b) final.

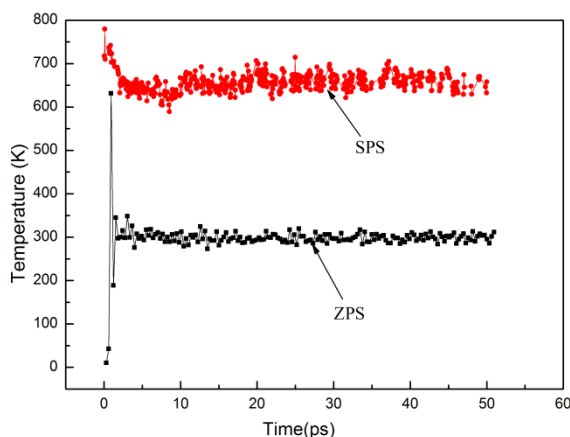


Figure 7. Temperature fluctuation curve of adsorption model of ZPS and SPS on Cu(111).

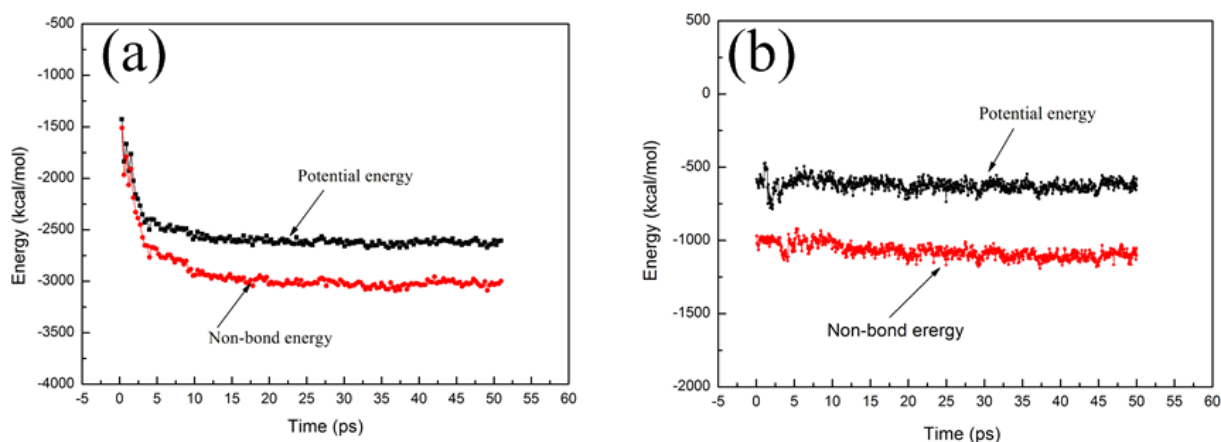


Figure 8. Energy fluctuation curve of adsorption model of (a) ZPS and (b) SPS on Cu(111).

The entire adsorption process of ZPS and SPS lasted for 7 and 3 ns, respectively. ZPS and SPS were completely parallel to the copper surface, covering the active position; thus, they played a role in controlling the plating speed and stabilizing the bath (see Figs. 5b and 6b). According to the equilibrium configuration of the two accelerators adsorbed on the Cu(111) surface, we concluded that both accelerators can be absorbed on the Cu surface through the -S-S- and benzothiazolyl group. Therefore, the hydrophilic groups were captured with copper ions in the plating solution. Furthermore, hydrophobic grouping cracked adsorbed on cathode surface, this conclusion coincides with [18]. Therefore, the accelerators were achieved by the two factors. We concluded that the accelerator molecules will form an adsorption layer on the Cu surface after being added to the solution.

Given the energy produced during the adsorption process of the accelerators, the velocity of the accelerator molecules will gradually decrease and eventually stop on the copper surface of the adsorbent medium. Thus, a part of the energy will be released due to the reduced velocity of motion, This part of the energy is called the adsorption energy ($E_{\text{adsorption}}$) of the accelerator on the copper surface. The calculation results are shown in Table 2.

Table 2. Interaction and binding energy of the two accelerators on the Cu(111) surface.

Additives	E_{complex} (kcal/mol)	$E_{\text{adsorption}}$ (kcal/mol)	E_{binding} (kcal/mol)
ZPS	403.68	-267.08	267.08
SPS	391.25	-275.96	275.96

As can be seen, the larger the adsorption energy value of SPS, the easier the adsorption of the accelerator on the surface and the higher the accelerator efficiency. SPS and ZPS have high adsorption energies. Therefore, calculating the energy can be used as an effective method for evaluating the performance and provide a reference for the kinetic parameter of electroplating. SPS has greater accelerator efficiency compared with ZPS, and this finding was consistent with the experiment results.

3.5. Quantum chemical calculations

The accelerators have analogous structures but show significantly different electrochemical behaviors for microvia filling in Cu electroplating. To reveal the relationship between the molecular structure of ZPS/SPS and their electrochemical behaviors, we performed quantum chemical calculations for orbital information and electronic properties [17].

Fig. 9 shows the localization of HOMO and LUMO of ZPS and SPS. The formation of a transition state was caused by an interaction between frontier orbitals (HOMO and LUMO) of reacting species according to the frontier molecular orbital theory [30]. Based on this theory, higher energy of HOMO (E_{HOMO}) is often linked with a stronger electron donating ability, and lower energy of LUMO (E_{LUMO}) is related to a stronger electron-accepting ability [37, 38]. The adsorption ability of the additives to the Cu surface should be accompanied by an increase in E_{HOMO} and a decrease in E_{LUMO} .

Hence, the energy gap ΔE ($\Delta E = E_{\text{LUMO}} - E_{\text{HOMO}}$) was used as an indicator to describe the adsorption ability of the organics to the metal surface [16, 17]. Table 3 lists the E_{HOMO} , E_{LUMO} , and ΔE of additives calculated by the orbital energy. Compared with ZPS (3.557 eV), SPS possessed higher ΔE (4.213 eV), Lei [17] concluded that ΔE was negatively correlated with the largest deposition potential change ($\Delta\eta$), illustrating the adsorption of SPS on the cathodic surface and the relatively stronger acceleration on copper electrodeposition. We found that consistent result of the SPS accelerator is more effective enhance Cu^+ formation [41]. In this study, we used $\eta_{\text{Cu}} = 0.0005$ eV/mol to compute for the number of transferred electrons. Table 3 shows that the softness of SPS was very close to that of Cu, and it was easier to combine with Cu. This finding indicates that soft acid coordinates with Cu^{2+} , which has empty d orbitals. The orbitals can be used as π bond of some d electrons of soft acid metal ions.

Table 3. Quantum Chemical Parameters Calculated at the B3LYP/ DFT Level for the protonated ZPS and SPS.

Additives	E_{HOMO} (ev)	E_{LUMO} (ev)	ΔE (ev)	η (ev/mol)	S(ev/mol)
ZPS	-5.760	-2.203	3.557	1.7785	0.2811
SPS	-5.877	-1.664	4.213	2.1115	0.2373

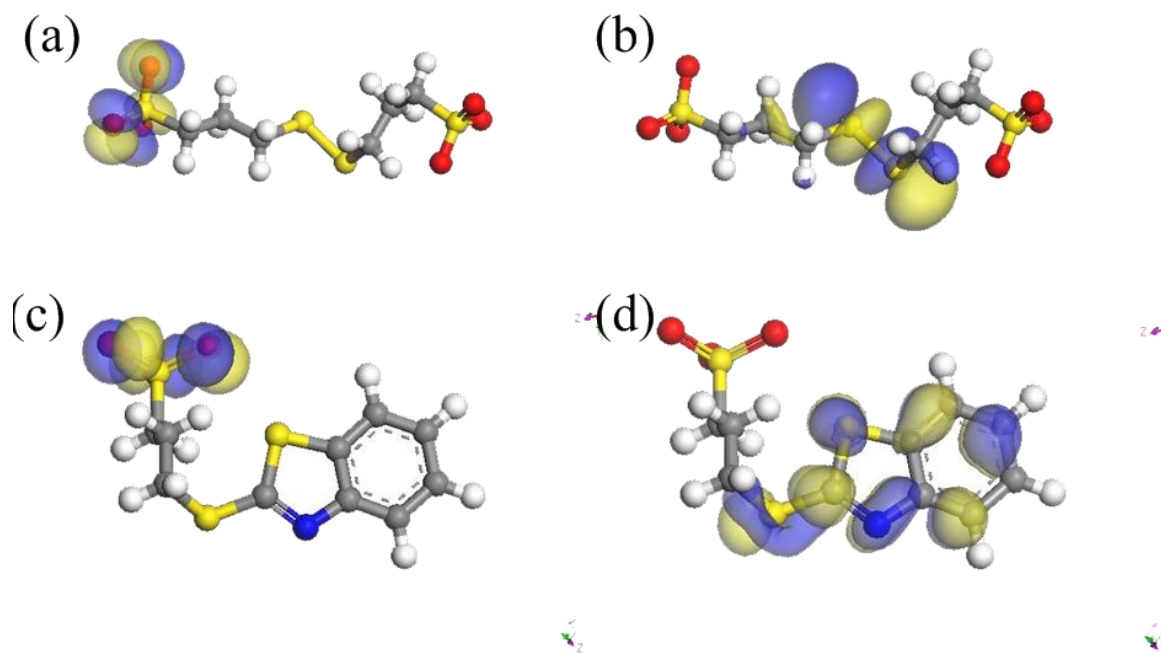


Figure 9. Frontier molecular orbital density distributions of optimized structure. ZPS (a) HOMO and (b) LUMO. SPS (c) HOMO and (d) LUMO.

The Fukui functions of ZPS and SPS were calculated to localize the nucleophilic and electrophilic sites (susceptible regions) in their molecular structure. The f^- and f^+ describe the ability for electrophilic and nucleophilic attack [16]. The atom with the highest f^- and f^+ values in the molecular structure was the most susceptible site for the electrophilic and nucleophilic attacks, respectively.

Table 4. Fukui indices (f^+ and f^-) of oxygen and sulphur atoms for SPS and ZPS.

Additives	Atom	f^+ (e)	f^- (e)
SPS	S(5)	0.012	0.277
	S(6)	0.030	0.275
	S(10)	0.094	-0.010
	O(14)	0.148	0.045
	O(15)	0.159	0.032
ZPS	S(5)	0.111	0.015
	S(7)	0.096	0.004
	O(15)	0.041	0.231
	O(16)	0.059	0.288

Fig. 9 shows the frontier molecule orbital density distributions (HOMO and LUMO) of the additives of ZPS and SPS. ZPS was mainly distributed on the aromatic ring region, whereas SPS was concentrated on the sulfonic group and disulfide bond. The aromatic ring region of ZPS was the likely reactive site for the adsorption of ZPS. By contrast, the disulfide bond of SPS was the likely reactive site

for the adsorption of SPS on the copper surface. The f^- and f^+ of O and S atoms located in the additives were calculated using Fukui function [16], and the results are listed in Table 4. So the higher the f^+ value, the easier the nucleophilic reaction occurs. By contrast, the higher the f^- value, the easier the electrophilic reaction occurs. The active sites were in accordance with the analysis above.

4. CONCLUSIONS

The introduction of a sulfhydryl group into polydisulfide could increase the polarization of the plating bath and improve the current density distribution in the pore and the ability for deep plating. This finding suggested that the underlying mechanism of ZPS was actually similar to that of SPS depolarizers. The results of electrochemical studies showed that 2.0 mg/L of SPS and 3.0 mg/L of ZPS were optimal concentrations for Cu electroplating. The MD simulation results showed that the two additives can be adsorbed on the Cu surface through the disulfide bond and benzothiazolyl with the alkyl chain approximately parallel to the surface. Quantum chemistry calculation results showed that the disulfide bond and benzothiazolyl are the active sites of the two additives. ZPS and SPS can be adsorbed on the Cu surface firmly by donating unoccupied orbital to Cu atoms and accepting electrons from 3d orbitals of Cu atoms. The accelerator provides the soliton electron pair to form the coordination bond with the hollow orbits of copper. Electrochemical studies and MD simulation can be used as an effective method for evaluating the performance of additives, and the results can provide a reference for predicting new additives for electroplating.

ACKNOWLEDGEMENTS

This work was financially supported by National Natural Science Foundation of China (No. 51604042, 51774051, 31527803, 21275022, 21545010 & 21501015).

References

1. R. M. Guijt, J. P. Armstrong, E. Candish and V. Lefleur, *Sens. Actuators, B*, 1 (2011) 307.
2. J. Vanfleteren, M. Gonzalez, F. Bossuyt and Y.Y. Hsu, *Mater. Res. Bull.*, 32 (2012) 54.
3. X. Li, J. Zang, Y. Liu, Z. Lu, Q. Li and C. M. Li, *Anal. Chim. Acta*, 10 (2013) 102.
4. Y. E. Sknar, N. V. Amirulloeva, I. V. Sknar and F. I. Danylov, *Mater. Sci.*, 3 (2016) 396.
5. Y. S. Wang, W. H. Lee, S. C. Chang, J. N. Nian and Y. L. Wang, *Thin Solid Films*, 1 (2013) 157.
6. C. E. Ho, C. W. Liao, C. X. Pan, H. J. Chen, J. C. Kuo and D. Chen, *Thin Solid Films*, 544 (2013) 412.
7. C. Wang, J. Q. Zhang, P. X. Yang and M.Z. An, *Int. J. Electrochem. Sci.*, 11 (2012) 10644.
8. Z. Lai, S. Wang, C. Wang, Y. Hong, Y. Chen, H. Zhang, *Electrochim. Acta*, 273 (2018): 318-326.
9. T. P. Moffat, D. Josell, *Isr. J. Chem.*, 50 (2010) 312.
10. T. P. Moffat, D. Wheeler, M. D. Edelstein and D. Josell, *IBM J. Res. Dev.*, 49 (2005) 19.
11. T. P. Moffat, D. Wheeler, D. Josell, *Electrochem. Soc. Interface*, 49 (2004) 46.
12. T. P. Moffat, D. Wheeler, D. Josell, *ECS Trans.*, 13 (2008) 129.
13. T. P. Moffat, D. Wheeler, S. K. Kim and D. Josell, *Electrochim. Acta*, 53 (2007) 145.

14. T. P. Moffat, D. Wheeler, S. K. Kim and D. Josell, *Electrochem. Soc. Interface*, 153 (2006) C127.
15. T. P. Moffat, D. Wheeler, W. H. Huber and D. Josell, *Electrochem. Solid-State Lett*, 4 (2001) C26.
16. B. Chen, J. Xu, L. Wang, L. Song, *ACS Appl. Mater. Interfaces*, 8 (2017) 7793.
17. Z. Lei, L. Chen, W. Wang, Z. Wang, C. Zhao, *Electrochim. Acta*, 178 (2015) 546.
18. S.W. Xia, M. Qiu, L.M. Yu, F.G. Liu, H.Z. Zhao, *Corros. Sci.*, 7 (2008) 2021.
19. J. J. Yan, L. C. Chang, C. W. Lu, W. P. Dow, *Electrochim. Acta*, 109 (2013) 1.
20. W. Luo, Z. P. Chen, J. H. Zhang, Y. Zhu, L. M. Gao, *J. Electrochem. Soc.*, 163.13 (2016): D694-D706.
21. A. Wang, B. Chen, L. Fang, J. Yu, L. Wang, *Electrochim. Acta*, 108 (2013): 698-706.
22. Z. Zhou, H. Cheng, L. Xue, J. Guan, *Materials Review*, 2 (2006) 79.
23. L. M. Rodriguez-Valdez, A. Martínez-Villafañ, *J. Mol. Struct.*, 713.1-3 (2005) 65.
24. H. H. H. Homeier, *J. Mol. Struct-Theochem*, 368 (1996): 81-91.
25. S. Manzetti, T. Lu, *J. Phys. Org. Chem.*, 26.6 (2013) 473.
26. R. G. Pearson, *Inorg. Chem.*, 27.4 (1988) 734.
27. M. D. Esrafil, R. Nurazar, V. Masumi, *Surf. Sci.*, 637 (2015) 69.
28. T. Düren, Y. S. Bae, R.Q. Snurr, *Chem. Soc. Review*, 28 (2009) 1237.
29. C. Wang, M. An, P. Yang, J. Zhang, *Electrochem. Commun.*, 18 (2012) 104.
30. M. F. Russo. Jr, R. Li, M. Mench, ACT. Van. Duin, *Int J Hydrogen Energy*, 36 (2011) 5828.
31. S. Xia, M. Qiu, L. Yu, F. Liu, H. Zhao, *Corros. Sci.*, 50 (2008) 2021.
32. M. F. Russo. Jr, ACT. Van. Duin, *Nucl. Instrum. Methods Phys. Res., Sect. B*, 269 (2011) 1549.
33. B. Behzadian, D. L Piron, C. Fan, J. Lessard, *Int. J. Hydrogen Energy*, 16.12 (1991): 791-796.
34. B. Xu, W. Yang, Y. Liu, X. Yin, W. Gong, Y. Chen, *Corros. Sci.*, 78 (2014): 260-268.
35. D. Wang, B. Xiang, Y. Liang, S. Song, C. Liu, *Corros. Sci.*, 85 (2014): 77-86.
36. P.T. Lee, Y.S. Wu, P.C. Lin, C.C. Chen, W.Z. Hsieh, C.E. Ho, *Surf. Coat. Tech.*, 320 (2017): 559-567.
37. T. C. Chen, Y. L. Tsai, C. F. Hsu, W.P. Dow, Y. Hashimoto, *Electrochim. Acta*, 212 (2016) 572.
38. M. A. Chidiebere, E. E. Oguzie, L. Liu, Y. Li, F. Wang, *Mater. Chem. Phys.*, 156 (2015): 95-104.
39. E. E. Oguzie, S.G. Wang, Y. Li, *J. Phys. Chem. C*, 113 (2009) 8420.
40. A. Kokalj, S. Peljhan, *Langmuir*, 26 (2010) 14582.
41. P. M. Vereecken, R. A. Binstead, H. Deligianni, P. C. Andricacos, *IBM J. RES. & DEV.*, 1 (2005) 49.

© 2019 The Authors. Published by ESG (www.electrochemsci.org). This article is an open access article distributed under the terms and conditions of the Creative Commons Attribution license (<http://creativecommons.org/licenses/by/4.0/>).